Acta Crystallographica Section D
Biological Crystallography
ISSN 0907-4449

Structure of a human IgA1 Fab fragment at 1.55 Å resolution: potential effect of the constant domains on antigen-affinity modulation

Agustin Correa,[a]‡ Felipe Trajtenberg,[b]‡ Gonzalo Obal,[c] Otto Pritsch,[c,d] Guillermo Dighiero,[a] Pablo Oppezzo[a] and Alejandro Buschiazzo[b,e]*

[a]Unit of Recombinant Proteins, Institut Pasteur de Montevideo, 11400 Montevideo, Uruguay, [b]Unit of Protein Crystallography, Institut Pasteur de Montevideo, 11400 Montevideo, Uruguay, [c]Unit of Protein Biophysics, Institut Pasteur de Montevideo, 11400 Montevideo, Uruguay, [d]Department of Immunobiology, Universidad de la Republica, 11800 Montevideo, Uruguay, and [e]Department of Structural Biology and Chemistry, Institut Pasteur, 75015 Paris, France

‡ These authors contributed equally to this work.

Correspondence e-mail: alebus@pasteur.edu.uy

Received 25 September 2012
Accepted 27 November 2012

PDB References: FabA, 3m8o; 3qnx; 3qny; FabG, 3qo1; FabG–peptide complex, 3qnz

Despite being the most abundant class of immunoglobulins in humans and playing central roles in the adaptive immune response, high-resolution structural data are still lacking for the antigen-binding region of human isotype A antibodies (IgAs). The crystal structures of a human Fab fragment of IgA1 in three different crystal forms are now reported. The three-dimensional organization is similar to those of other Fab classes, but FabA1 seems to be more rigid, being constrained by a hydrophobic core in the interface between the variable and constant domains of the heavy chain (V_H–C_{H1}) as well as by a disulfide bridge that connects the light and heavy chains, influencing the relative heavy/light-chain orientation. The crystal structure of the same antibody but with a G-isotype C_{H1} which is reported to display different antigen affinity has also been solved. The differential structural features reveal plausible mechanisms for constant/variable-domain long-distance effects whereby antibody class switching could alter antigen affinity.

1. Introduction

Immunoglobulins (Igs) are heterodimeric proteins composed of two heavy (H) and two light (L) chains, each containing a variable (V) domain that defines the antigen (Ag) binding site as well as several constant (C) domains that essentially have effector functions. Both variable V_H and V_L domains contain three regions of particularly high sequence variability termed complementarity-determining regions (CDRs). Four regions of higher sequence conservation, termed framework regions (FRs), create a scaffold that surrounds, and can also affect, the structure of the CDRs as a second shell of influence. The three L-chain CDRs, juxtaposed with the three CDRs on the H chain, are mostly included in exposed loops that connect particular β-strands of the variable Ig domains, forming the antigen-combining site (Al-Lazikani *et al.*, 1997; Mariuzza & Poljak, 1993; Poljak, 1991). CDRs are thus classically accepted as the main contributors to determining Ag specificity and affinity through their relative orientation, their variable amino-acid sequence and the precise conformation of their constitutive residues (Ramsland & Farrugia, 2002).

A most important feature of antibodies is their ready classification into five different isotypes, as defined by their H-chain constant domains (C_H), through a genetic process known as isotype- or class-switch recombination (CSR). This change not only affects the effector functions but also determines the half-life and tissue localization of the antibodies. Given that CSR leaves the V domains intact, it has been assumed that CSR alters effector functions without affecting the specificity and the affinity of the Ag–antibody interaction (Tonegawa, 1983).

Among the different classes, IgA is the most abundant antibody (Ab) in humans and is the dominant isotype in mucosal regions, which represent the primary avenue for invasion by many pathogens. Mucosal immunity prevents pathogen adherence by secretory IgA-mediated exclusion and systemic immune effector functions through the action of serum Abs. IgA is also the most heterogeneous human Ab class, occurring in several molecular forms. The monomeric form is similar to IgG and IgE but contains an additional carboxy-terminal tail piece that interacts with the joining chain. The dimeric form results from the association of two IgA chains through the joining region. Finally, the secreted form is the consequence of the addition of cleaved polymeric Ig (pIg) receptor ectodomain to dimeric IgA (Hanson & Brandtzaeg, 1993; Brandtzaeg *et al.*, 1999). Moreover, two allotypic subclasses exist (IgA1 and IgA2), as well as different glycoforms. In sera, IgA is predominantly in a monomeric state, whereas in mucosal surfaces it is mainly polymeric and is found as dimeric IgA covalently linked to the secretory component. Interestingly, IgA1 has only been found in humans and great apes, as opposed to other mammals, where the single occurring IgA is more similar to the human IgA2 subclass (Kaetzel, 2005).

Despite the biological relevance of IgAs, few structural data are currently available. Fairly recently, the structure of the Fc fragment of human IgA1 was first determined by X-ray crystallography (Herr *et al.*, 2003) only after being complexed with the ectodomain of its cognate receptor FcαRI or the superantigen-like protein SSL7 from *Staphylococcus aureus* (Ramsland *et al.*, 2007); the unbound Fcα proved recalcitrant to crystallization on its own. These models remain the only sources of medium-resolution experimental data corresponding to human IgA. Low-resolution models of IgA1 and IgA2 have been proposed on the basis of small-angle X-ray scattering, analytical centrifugation and homology modelling (Boehm *et al.*, 1999; Furtado *et al.*, 2004; Almogren *et al.*, 2006), but cannot be used for detailed atomic-level analyses. As for the antigen-binding fragment of the IgA (FabA), to the best of our knowledge no three-dimensional structure of human FabA has been reported. Although pepsin-digested mouse IgA has long been known to render crystallizable Fab fragments (Inbar *et al.*, 1971), only two different murine monoclonal Fab crystal structures have since been reported (Segal *et al.*, 1974; Suh *et al.*, 1986).

In contrast to IgA2, human IgA1 has a relatively long hinge region of 23 amino acids rich in proline and carrying between three and five O-linked sugars attached to Thr and Ser residues (Mattu *et al.*, 1998; Royle, 2006; Iwasaki *et al.*, 2003; Yoo & Morrison, 2005). This hinge region is susceptible to specific cleavage by IgA proteases. These proteolytic enzymes (Mulks & Shoberg, 1994) are secreted by a number of pathogenic bacterial species such as *Neisseria meningitidis*, *N. gonorrhoeae*, *Haemophilus influenzae*, *Clostridium ramosum*, *Streptococcus pneumoniae* and *S. sanguis*, which are typically adapted to mucosal surface colonization.

We have previously analyzed four different human monoclonal antibodies of different isotypes (IgA1κ, IgG1κ, IgG2κ and IgG4κ) isolated from the serum of a lymphoplasmocytic lymphoma patient (Houdayer *et al.*, 1993). We now report high-resolution crystal structures of the human IgA1κ antigen-binding fragment determined in three different crystal forms. To the best of our knowledge, this constitutes the first crystallographic structure of a human IgA Fab to be disclosed. Comparative analyses with previously reported IgG structures uncover plausible clues pointing to structural differences in the V_H–C_{H1} interfaces as well as to overall differential rigidity of the C_{H1} domains. The assumption that only the variable domains in Igs control antigen-binding affinity/specificity has received challenging evidence, mostly on thermodynamic and kinetic grounds. Different isotype antibodies sharing identical V domains can display significant differences in affinity or specificity towards their cognate Ag, suggesting that the CH regions are able to affect the structure of the Ag binding site (Cooper *et al.*, 1993; Dam *et al.*, 2008; McLean *et al.*, 2002; Pritsch *et al.*, 1996, 2000; Torres & Casadevall, 2008; Torres *et al.*, 2005, 2007*a*,*b*). Apart from the IgA1κ that we have crystallized in this work, the other isotypic variants from the same patient share identical V_H and V_L domains. It has been shown that full immunoglobulins as well as Fab fragments of IgA1κ and IgG1κ display different affinities towards purified tubulin (Pritsch *et al.*, 1996). The reactive β-tubulin epitope was subsequently identified and surface plasmon resonance experiments confirmed differential affinities when comparing whole IgA1 and IgG1 molecules against the synthetic peptidic epitope (Pritsch *et al.*, 2000). As a further step in elucidating the structural bases for such effects, we solved the crystal structure of the IgG1κ form, lending further support to the notion that molecular rigidity/flexibility may exert long-distance effects.

2. Materials and methods

2.1. Production and purification of *N. gonorrhoeae* and *C. ramosum* IgA proteases

The IgA protease gene from *N. gonorrhoeae* was PCR-amplified from genomic DNA (*N. gonorrhoeae* strain FA19) using the primers GonoFor, 5′-AAACATATGGCATTGG-TGAGAGACGATGTGC-3′, and GonoRev, 5′-ACCCTC-GAGTTACGGGGCCGGCTTGACTGGG-3′. PCR was performed with high-fidelity *Pfu* polymerase (Stratagene) according to the manufacturer's instructions. The primers were designed to add *Nde*I and *Xho*I restriction sites for subsequent cloning into the expression vector pET28a (Novagen). PCR cycling took place as follows: denaturation at 367 K for 4 min followed by 28 cycles of denaturing at 367 K for 1 min, annealing at 335 K for 1 min and extension at 345 K for 4 min, with a final extension step at 345 K for 10 min. The vector and PCR fragments were digested with *Nde*I and *Xho*I, ligated and transformed into *Escherichia coli* XL1-Blue electrocompetent cells. Colonies harbouring the correct recombinant plasmid were identified by restriction analyses. Recombinant protein expression was subsequently performed

with *E. coli* BL21 (DE3) pLysS in autoinduction medium (Studier, 2005) for 20 h at 293 K.

In the case of the IgA protease from *C. ramosum*, a pQE60 (Qiagen) plasmid carrying the gene was kindly provided by Dr Knud Poulsen (Kosowska *et al.*, 2002) and protein expression was performed in *E. coli* M15[pREP4] cells in 2×YT medium. Induction was triggered with 1 m*M* IPTG when the cell cultures reached an A_{600} of 0.7; they were then incubated at 298 K for a further 7 h before cell harvesting.

For both proteases, the cells were centrifuged at 5000*g* after induction, resuspended in 50 m*M* Tris–HCl pH 8.0, 500 m*M* NaCl, 20 m*M* imidazole, 1 mg ml^{-1} hen egg-white lysozyme and further disrupted by mild sonication. The supernatants were purified by immobilized metal Ni^{2+}-affinity chromatography (HisTrap HP column, GE Healthcare) and subsequently by gel-filtration chromatography on a Superdex 200 16/60 column (GE Healthcare) pre-equilibrated with either 50 m*M* Tris–HCl pH 7.5, 500 m*M* NaCl for the *N. gonorrhoeae* protease or 50 m*M* Tris–HCl pH 8.2, 150 m*M* NaCl for the *C. ramosum* protease.

2.2. Purification of antibodies

The Fab fragments used in the present work were obtained from the serum of a patient, PER, affected by an immunocytic lymphoma expressing four different clonally related immunoglobulins (Dighiero *et al.*, 1982; Houdayer *et al.*, 1993). The immunoglobulins were purified from the sera by ammonium sulfate precipitation (47% saturation) and were resuspended in 5 m*M* Na_3PO_4 pH 7.5; this was followed by anion-exchange chromatography on a DEAE-Sepharose column. Two different IgGs (γ_1 and γ_2 subclasses) were eluted from the DEAE-Sepharose at the same ionic strength (0.005 *M*) and were further isolated by cation-exchange chromatography on a Resource S column (GE Healthcare) equilibrated with 100 m*M* HEPES pH 7.1. IgG_4 was eluted in the 0.045 *M* DEAE fraction and the dimeric and monomeric forms of IgA1 were obtained from the DEAE-Sepharose after applying 1 *M* NaCl. The dimeric IgA1 was further purified by size-exclusion chromatography on a Superdex 200 26/60 column (GE Healthcare) pre-equilibrated with 20 m*M* Tris–HCl pH 7.5, 50 m*M* NaCl.

2.3. Generation and purification of FabA fragments with different glycosylation patterns from human IgA1

The human dimeric IgA1 was cleaved with the IgA proteases at an enzyme:substrate ratio of 1:5 for 20 h at 310 K in 50 m*M* Tris–HCl pH 8.0, 50 m*M* NaCl. Either 0.5 m*M* EDTA or 50 µ*M* $ZnSO_4$ was added for subsequent cleavage with the IgA proteases from *N. gonorrhoeae* or *C. ramosum*, respectively. After cleavage, the Fab fragments were purified by gel filtration on a Superdex 75 16/60 column (GE Healthcare) pre-equilibrated with 20 m*M* Tris–HCl pH 7.5, 50 m*M* NaCl.

2.4. Generation and purification of IgG1κ Fab fragments

IgG1 Fab fragments were obtained following a 3 h digestion at 310 K with papain (Sigma) at an enzyme:substrate ratio of 1:40 in the presence of 10 m*M* cysteine and 10 m*M* EDTA. The proteolytic reaction was stopped with 30 m*M* iodoacetamide. After buffer exchange to 20 m*M* Na_3PO_4 pH 7.1 using a HiPrep Desalting 26/10 column (GE Healthcare), the sample was charged onto a cation-exchange Resource S column (GE Healthcare) and final purification was achieved by size exclusion using a Superdex 75 column (GE Healthcare) pre-equilibrated with 20 m*M* Tris–HCl pH 7.5, 50 m*M* NaCl.

2.5. Protein crystallization

Purified Fab samples were used to screen for crystallization conditions in a 96-well sitting-drop vapour-diffusion setup (Greiner plates) assisted by a Honeybee 963 robotic station (Digilab). Drops were set up with 250 nl protein solution and 250 nl reservoir solution and were equilibrated against 100 µl reservoir solution. Initial hits were subsequently optimized manually using a hanging-drop setup in 24-well VDX plates (Hampton Research) at 297 K.

In the case of FabA, three different crystal forms were ultimately used throughout. Monoclinic form *A* crystals (space group $P2_1$, 2.3 Å resolution) grew from 2 µl protein solution at 16.3 mg ml^{-1} mixed with an equal volume of reservoir solution consisting of 0.2 *M* potassium sulfate, 20% PEG 3350. These crystals were cryoprotected with 25% glycerol, 0.1 *M* potassium sulfate, 20% PEG 3350 and flash-cooled in liquid N_2 until diffraction setup. Monoclinic form *B* crystals (space group $P2_1$, 1.55 Å resolution) were used directly from the Greiner plates; the mother liquor consisted of 0.2 *M* NaCl, 0.1 *M* Tris–HCl pH 7, 30% PEG 3000 and the protein was used at a starting concentration of 13.6 mg ml^{-1}. Cryoprotection was achieved with modified mother liquor that included a final concentration of 15% glycerol. Finally, the orthorhombic form crystals (space group $P2_12_12$, 2.4 Å resolution) grew from 2 µl protein solution at an initial concentration of 10 mg ml^{-1} mixed with 2 µl reservoir solution consisting of 1.8 *M* ammonium sulfate, 0.1 *M* sodium phosphate/sodium citrate pH 3.8. To obtain higher quality crystals, the first crystals to grow were used as seeds in fresh drops following standard streak-microseeding techniques. Cryoprotection of the orthorhombic crystals was performed with the same mother-liquor composition but with the addition of glycerol to a final concentration of 21.6%.

Crystallization of FabG was achieved in two ways: as free protein or in cocrystallization setups with the epitope peptide. The apo crystals were optimized in VDX plates using a hanging-drop setup. They grew in space group $P2_1$ using 2 µl protein solution at 25 mg ml^{-1} mixed with an equal volume of 0.1 *M* sodium citrate pH 5.5, 20% 2-propanol, 16% PEG 4000. These crystals were cryoprotected with identical mother liquor with an additional 15% glycerol prior to liquid-N_2 flash-cooling. The peptide complex was obtained by co-incubating FabG at 25 mg ml^{-1} with a ten-residue peptide derived from human β-tubulin at 3.25 mg ml^{-1} (synthetic peptide sequence

Table 1
X-ray diffraction data-collection and refinement statistics.

Values in parentheses are for the highest resolution shell.

	FabA			FabG	
	Orthorhombic	Monoclinic form *A*	Monoclinic form *B*	Apo	Peptide complex
Crystal parameters					
Space group	$P2_12_12$	$P2_1$	$P2_1$	$P2_1$	$P2_12_12_1$
Unit-cell parameters (Å, °)	a = 49.8, b = 95.8, c = 107.3	a = 96.3, b = 50.0, c = 99.2, β = 107.5	a = 43.8, b = 76.3, c = 55.8, β = 105.5	a = 53.3, b = 67.2, c = 68.9, β = 103.4	a = 53.4, b = 66.4, c = 137.7
Data collection					
Resolution (Å)	49.7–2.20 (2.32–2.20)	35–2.30 (2.40–2.30)	19.2–1.55 (1.59–1.55)	20–2.40 (2.53–2.40)	28.2–2.20 (2.32–2.20)
Wavelength (Å)	1.5418	1.5418	1.5418	1.5418	1.5418
Measured reflections	94610	140791	168232	61325	88143
Multiplicity	3.5 (3.5)	3.5 (3.3)	3.3 (2.9)	3.3 (3.3)	3.4 (3.4)
Completeness (%)	100 (100)	97.3 (91.2)	98.1 (88)	99.7 (100)	99.9 (100)
$R_{\rm meas}$† (%)	12.3 (58)	7.6 (52.7)	4.6 (20.5)	10.9 (59.1)	8.8 (58.6)
$\langle I/\sigma(I)\rangle$	9.8 (2.6)	13.4 (3.1)	19.5 (6.8)	11.2 (2.7)	14 (2.6)
Refinement					
Resolution (Å)	18.15–2.20	18.75–2.30	19.2–1.55	19.3–2.40	28.2–2.20
$R_{\rm cryst}$‡	0.181	0.187	0.153	0.166	0.198
No. of reflections for $R_{\rm cryst}$	25419	38235	48695	17729	24390
$R_{\rm free}$‡	0.224	0.218	0.182	0.224	0.235
No. of reflections for $R_{\rm free}$	1352	1220	1554	879	1203
R.m.s.d. stereochemistry§					
Bond lengths (Å)	0.01	0.01	0.008	0.01	0.01
Bond angles (°)	1.22	1.24	1.25	1.28	1.25
Other model properties and validation statistics					
Protein non-H atoms	3296	6307	3671	3301	3220 [3201 protein/19 Ag peptide]
Water atoms	234	245	591	185	104
Ligand atoms	18 [3 glycerol]	12 [2 glycerol]	22 [3 glycerol/4 Cl^-]	12 [2 glycerol]	6 [1 glycerol]
Average B factor (Å^2)	33.8	50.2	16.1	32.0	34.7
Ramachandran plot statistics					
Favoured	422	824	428	424	410
Allowed	11	20	12	10	10
Disallowed	1	2	0	0	0
PDB code	3qnx	3qny	3m8o	3qo1	3qnz

† $R_{\rm meas} = \sum_{hkl}\{N(hkl)/[N(hkl)-1]\}^{1/2}\sum_i |I_i(hkl) - \langle I(hkl)\rangle|/\sum_{hkl}\sum_i I_i(hkl)$, where $N(hkl)$ is the multiplicity for each reflection, $I_i(hkl)$ is the intensity of the ith observation of reflection hkl and $\langle I(hkl)\rangle$ is the mean of the intensity of all observations of reflection hkl. ‡ $R = \sum_{hkl}||F_{\rm obs}| - |F_{\rm calc}||/\sum_{hkl}|F_{\rm obs}|$; $R_{\rm cryst}$ and $R_{\rm free}$ were calculated using the working and test reflection sets, respectively. § Calculated with *MolProbity* (Chen *et al.*, 2010).

TAEEEEDFGE; corresponding to residues 429–438 of β-tubulin 5; NCBI Reference NP_821133.1). Optimal crystals were ultimately obtained by mixing 2 µl of the complex solution with an equal volume of an identical mother liquor to that used for the apo protein. Mother liquor with 10% glycerol and 3.25 mg ml^{-1} peptide was used as a cryoprotectant.

2.6. Data processing and structure determination, refinement and analysis

Complete X-ray diffraction data sets were obtained using a standard single-crystal oscillation setup with a Cu rotating-anode generator (MicroMax-007 HF, Rigaku), multilayer optics (VariMax HF, Rigaku) and an image-plate detector (MAR345, MAR Research). Indexing and integration were performed with *XDS* (Kabsch, 2010) or *MOSFLM* (Leslie, 1992) and subsequent scaling and intensity reduction were performed with *SCALA* and *TRUNCATE* within the *CCP*4 suite of programs (Winn *et al.*, 2011).

For chronological reasons, the first structure determined corresponded to the monoclinic form *A* of FabA and provided a clear solution by molecular replacement using *AMoRe* (Trapani & Navaza, 2008). The search probe was a chimeric model generated by combination of the light chain of the humanized FabG KR127 (PDB entry 2eh7; Chi *et al.*, 2007) and the heavy chain of the mouse FabA J539 (PDB entry 2fbj; T. N. Bhat, E. A. Padlan & D. R. Davies, unpublished work). The high-resolution monoclinic form *B* was readily solved using a partially refined model of form *A* as the search model. The fully refined high-resolution model was finally used to solve the orthorhombic form by molecular replacement.

Apo FabG was solved in the monoclinic unit cell by molecular replacement with *AMoRe* using the complete model of FabG KR127 (PDB entry 2eh7) as a search probe. The orthorhombic complex was subsequently solved by molecular replacement using the refined apo FabG model.

Refinement proceeded smoothly in all cases in reciprocal space using the program *phenix.refine* (Adams *et al.*, 2010) iterated with real-space manual model rebuilding using *Coot* (Emsley & Cowtan, 2004). Once advanced in refinement according to model completeness and convergence in *R*-factor minimization, a simple translation–libration–screw (TLS) parameterization was included in each model, essentially by considering each immunoglobulin domain as a separate TLS body. Refinement of these TLS parameters was carried out as implemented in the program *phenix.refine* and systematic

comparisons of the inclusion or the absence of TLS parameterization were performed by monitoring the significant decrease in the *R* factors (particularly >0.5% in R_{free}). An improvement was indeed confirmed for the five different models; hence, TLS was maintained in the final refinement cycle (detailed descriptions of the TLS groups and final refined tensor values are included in the PDB headers under Remark 3). Total atomic displacement parameters (ADPs) are thus stored in the model ANISOU records and their isotropic equivalents are stored in the ATOM records. Full atomic anisotropic refinement of ADPs was attempted with the FabA monoclinic form *B*, which diffracted to 1.55 Å resolution (see Table 1), but no improvement in R_{free} was detected and it was thus abandoned (most probably owing to a borderline but insufficient data-to-parameter ratio). Prior to atomic coordinate deposition, validation and final corrections were guided using *MolProbity* (Chen *et al.*, 2010). Apart from visual inspection, structural analyses were performed using *BAVERAGE* (Winn *et al.*, 2011), *ESCET* (Schneider, 2000), *CASTp* (Dundas *et al.*, 2006), *Dom_Angle* (Su *et al.*, 1998) and *Adaptive Poisson–Boltzmann Solver* (*APBS*) for macromolecular electrostatic potential calculations (Baker *et al.*, 2001). Figures were prepared with *PyMOL* (DeLano, 2002).

3. Results

3.1. Generation of IgA Fab fragments with different glycosylation patterns

In an initial attempt to obtain IgA Fab (FabA) crystals, we used *N. gonorrhoeae* IgA protease (Fig. 1*a*). Despite evaluating 384 independent crystallogenesis conditions using these FabA fragments, we failed to obtain crystals. Considering the hypothesis that O-glycosylation in the hinge region could preclude crystal packing, we prepared a different FabA batch using the protease from *C. ramosum*, which generated a Fab fragment without the hinge region and hence free from any carbohydrate decoration (Fig. 1). Indeed, this form readily crystallized in three different crystal packings (Table 1).

3.2. IgA1κ Fab structure determination and overall description

Three different crystal structures corresponding to the Fab fragment of IgA1κ (FabA) were solved and refined (Table 1). In contrast to the situation with IgG Fabs, for which numerous experimental structures have been reported, there is a lack of FabA data to provide a sufficiently diverse sampling array for comparison. We were thus keen to obtain the FabA in different crystal forms, allowing more reliable comparative structural analyses that rule out crystal-packing effects.

The structures were determined by molecular replacement and refined to resolutions ranging from 1.55 to 2.4 Å (Table 1). The four independently refined Fab fragments (Fig. 2) share the canonical β-sandwich Ig fold with four domains: V_L, C_L, V_H and C_{H1} (where L indicates light chain, H heavy chain, V variable domain and C constant domain). The elbow angles vary between 142.2° and 144.6° and are well within the most typical values for antibodies with κ light chains (Stanfield *et al.*, 2006).

Although IgA N-glycosylation has been reported on the Fab portions (Mattu *et al.*, 1998), we did not observe any modified Asn residues in the electron-density maps, as was expected from the sequences, since no proper sequons were actually present (a single Asn-Pro-Ser motif is present within the FabA heavy chain, with Pro being inhibitory for N-glycosylation).

3.3. Differential structural features of FabA

While the orthorhombic form of FabA diffracted to 2.2 Å resolution, the other two crystals belonged to the monoclinic space group $P2_1$; one of them (monoclinic form *B*; Table 1) diffracted to near-atomic resolution (1.55 Å). Only the monoclinic form *A* displayed two Fab fragments per asymmetric unit; the other two crystals contained only one. The packings and solvent contents are quite different among the three structures. The resulting differential crystal contacts slightly alter the conformation of some loops, especially the CDR H3 loop, which is found to establish crystal contacts in the 1.55 Å resolution structure, showing signs of local conformational rearrangements.

As in other Igs, the variable and constant domains in this FabA are connected by a short and extended polypeptide known as the switch region. A closer analysis of this segment revealed two important features. On the one hand, a proline (Pro122) is observed in FabA, which is prone to induce a more rigid loop (Fig. 3*a*) when compared with the conserved

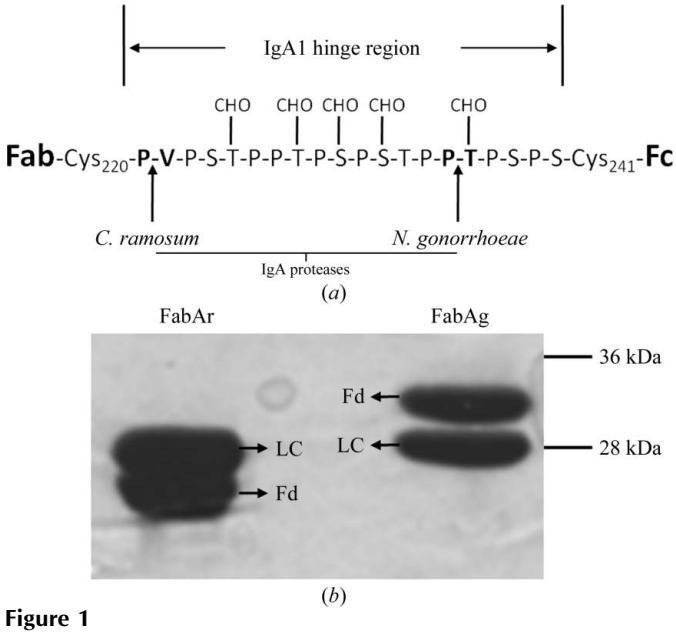

Figure 1
Proteolytic generation of FabA fragments with different glycosylation patterns. (*a*) Schematic representation of the human IgA1 hinge region. The O-glycosylation sites (CHO) and IgA-protease cleavage sites are indicated. Note the complete avoidance of final glycosylation when using the *C. ramosum* protease. (*b*) SDS–PAGE showing the purified FabA fragments after *C. ramosum* (FabAr) or *N. gonorrhoeae* (FabAg) proteolytic cleavage. LC, light chain; Fd, heavy-chain portion of the Fab fragment.

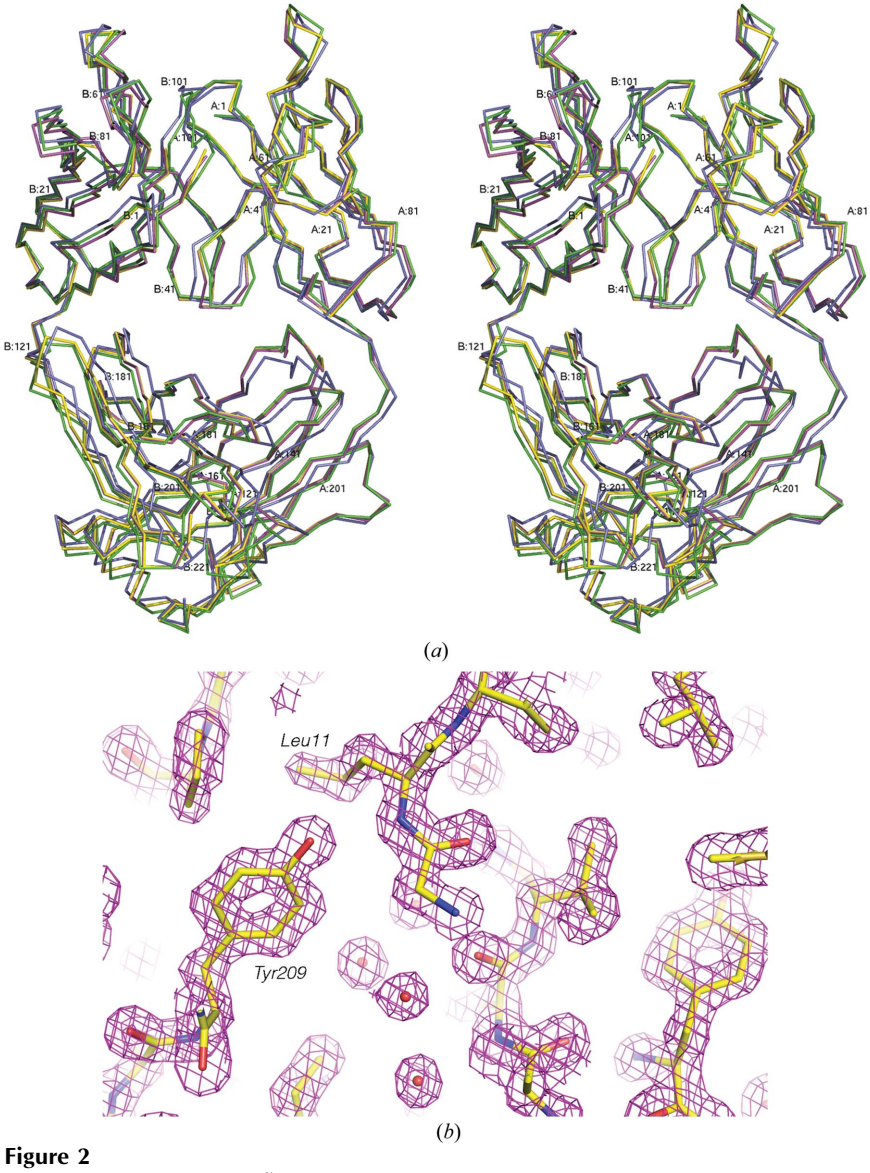

Figure 2
IgA1κ Fab structure. (*a*) C^{α} trace in diverging-eyed stereoview corresponding to the four independently refined FabA fragments after structural superposition. The orthorhombic form is shown in green, the monoclinic form *A* is shown in yellow and magenta for the two molecules in the asymmetric unit and the high-resolution monoclinic form *B* is shown in blue. Residue numbers are labelled every 20 amino acids; light-chain residues are marked A and heavy-chain residues are marked B. (*b*) σ_A-weighted $2mF_{obs} - DF_{calc}$ electron-density map of FabA (monoclinic form *B*) contoured at 1.3σ. The V_H–C_{H1} interfacing residues Leu11–Tyr209 are highlighted.

threonine that is found at this position in IgG Fabs (see Supplementary Fig. S1[1] for a multiple sequence alignment). Pro122 actually forms part of a local hydrophobic core that bridges the variable and constant regions in FabA: Ala120 and Pro122 in the switch loop, Tyr209, Phe151 and Pro152 in the C_{H1} domain, and Leu11, Thr116 and Ser118 in the V_H domain; all establish direct van der Waals contacts. On the other hand, this hydrophobic core is further stabilized by a hydrogen bond between the hydroxyl group of Tyr209 and the main-chain N atom of Leu11 (Fig. 3*a*). After performing a multiple structural alignment including human FabG1, FabM and FabE fragments, as well as mouse FabA, the abovementioned rigidity-inducing traits are only present in the human FabA that we report here (Fig. 3*b*).

With regard to the organization of disulfide bridges, Ig domains always display one conserved intrachain disulfide bond, which is indeed observed in each variable (Cys23–Cys93 in V_L and Cys22–Cys98 in V_H in the numbering of our model) and constant (Cys139–Cys199 in C_L and Cys145–Cys204 in C_{H1}) domain of this FabA. When compared with reported FabG1 structures, a few differential features can readily be identified in human IgA1 FabA, which displays two extra disulfide bridges: one intrachain bond in the heavy chain (Cys196–Cys220; also visible in mouse FabA; see, for example, PDB entry 2fbj) and one interchain bond (light chain Cys219–heavy chain Cys133; Fig. 3*c* and Supplementary Fig. S1). The latter is not only absent in IgG1 Fabs but also in human IgA2 (Chintalacharuvu *et al.*, 2002). In addition, mouse IgA lacks Cys133 altogether; hence, the corresponding loop between CHα β1 and β2 in the mouse molecule adopts a different conformation. This extra interchain disulfide bridge in FabA directly modulates the relative orientation of the light and heavy chains in the constant region.

3.4. Crystal structure of the related IgG1κ Fab

To go one step further in the analysis of this human IgA Fab fragment, we decided to solve the crystal structure of the Fab fragment from the related IgG1κ antibody purified from the serum of the same patient. It has previously been shown that despite sharing identical V domains, these two isotypic variants display different affinities for the antigenic epitope (Pritsch *et al.*, 1996). The apo IgG1 Fab fragment crystallized in a monoclinic space group ($P2_1$) and was refined to 2.4 Å resolution (Table 1). We also obtained its structure in complex with a synthetic ten-residue peptide including an antigenic epitope derived from β-tubulin; the cocrystals grew in a different space group ($P2_12_12_1$, 2.2 Å resolution) but shared a similar crystal packing as the apo form.

For unexplained reasons, the antigen did not bind to completion; it was only possible to observe three peptide amino acids in the electron-density maps, with a glutamate

[1] Supplementary material has been deposited in the IUCr electronic archive (Reference: RR5031). Services for accessing this material are described at the back of the journal.

clearly discernable at the centre position (Fig. 4*a*). Given the presence of several glutamates in the peptide sequence, with no further side chains confidently defined in the density, the sequence register cannot be ascertained. The antigen-binding crevice extends beyond the limits of the short bound peptidic segment, revealing a strong positive electrostatic potential when mapped onto the solvent-exposed surface (Fig. 4*b*). This corresponds well with its binding affinity towards an antigenic epitope particularly rich in negatively charged residues.

Polar and van der Waals interactions with the peptide can be identified involving the side chains of residues Asn33, His35 (CDR H1) and Arg101 CDR H3) in the heavy chain (Fig. 4). Two strong ionic bonds are also observed in this chain, bridging the defined glutamate of the peptide through its carboxylate group with Arg50 and Lys52 (CDR H2). A few residues on the light chain are observed to make additional interactions: O atoms on the side chain of Thr99 as well as on the main chain of Asn96 and Lys97 appear to be involved in polar interactions with the peptide, while Leu101 is observed to interact hydrophobically; all of these light-chain residues are included in CDR L3.

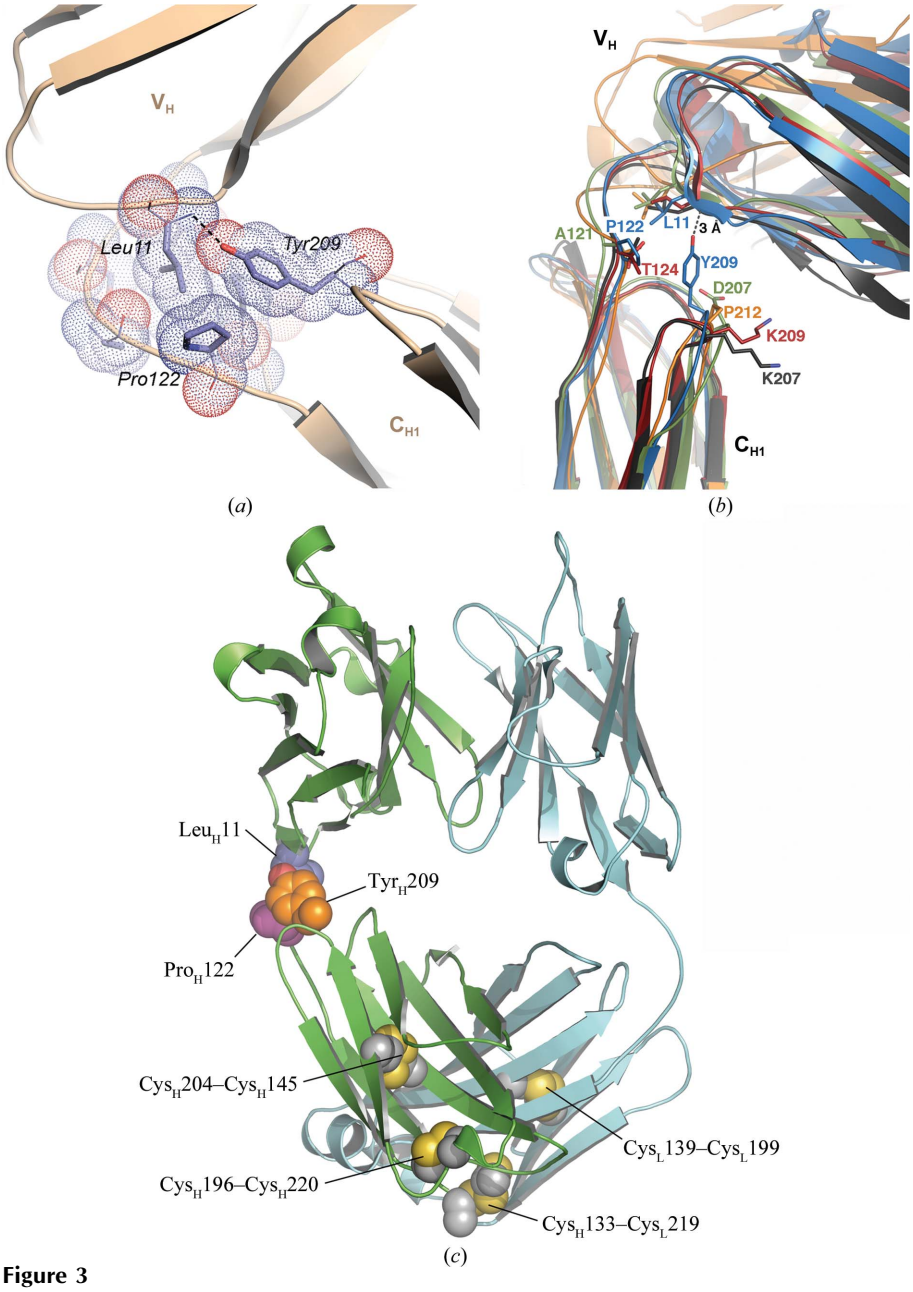

Figure 3
FabA-specific structural features. (*a*) Hydrophobic core linking the variable (V_H) and constant (C_{H1}) domains of the FabA heavy chain. The atomic volumes occupied by the seven residues in contact (details in the main text) are represented as dots; their side chains are represented as sticks and their main-chain atoms as lines. For clarity, only three are labelled; in particular, note the hydrogen bond between the OH group of Tyr209 and the main-chain N atom of Leu11 (dotted line). (*b*) Superposition of FabA (blue) with FabG1 (dark grey; this work; PDB entry 3qo1), human FabE (red; PDB entry 2r56), human FabM (orange; PDB entry 2agj) and mouse FabA (green; PDB entry 2fbj). While Leu11 in the VH domain is strictly conserved, note the presence of key residues Tyr209 and Pro122 in human IgA1 only (structurally equivalent residues are labelled according to model colour). In the hinge region, FabG1 Thr122 (homologous to FabE Thr124) and FabM Ala123 (equivalent to mouse FabA Ala121) are shown but are not labelled for the sake of clarity. (*c*) FabA viewed in a similar orientation as in Fig. 2(*a*), highlighting the location of the intra-chain disulfide bond Cys_L139–Cys_L199 in the light chain (cartoon coloured cyan) and the Cys_H145–Cys_H204 disulfide bond in the heavy chain (green), both of which are widely conserved among Igs. Human IgA1 FabA displays two extra bonds: the intra-chain Cys_H196–Cys_H220 in the heavy chain and the inter-chain Cys_L219–Cys_H133. The latter closes the inter-chain solvent-exposed cavity at the tip by bringing the C_{H1} loop closer to the light chain.

4. Discussion

To the best of our knowledge, high-resolution structures of human antigen-binding fragments of IgA have never been reported. We believe that this is linked to the heavy O-glycosylation present at the hinge region of this antibody isotype leading to heterogeneity and molecular flexibility, and eventually precluding crystallization. In support of this hypothesis, the identification of a proper proteolytic approach to generate FabA indeed allowed us to crystallize it in three different forms suitable for diffraction studies. This approach might open the way to perform broader high-resolution studies aimed at this highly relevant class of immunoglobulin molecules. Although similar to IgG Fabs overall, the structural details of IgA1 revealed a more rigid architecture constrained by both a hydrophobic core in the V_H–C_{H1} interface as well as a disulfide bridge connecting the light and heavy chains which is absent in both human IgA2 and mouse IgA. The

higher rigidity affects the differential interaction between the constant and variable portions of the Fabs, which may correlate *in fine* to antigen-binding affinity modulation. It is ever more clear that modulation of affinity in proteins can be intimately linked to conformational entropy, sometimes challenging simpler arguments based solely on discrete conformational rearrangements among states (Tzeng & Kalodimos, 2012).

These observations extend the current state of knowledge, strengthening the idea that entropy-driven energetic contributions, which are strongly influenced by molecular flexibility among other factors, have to be considered when predicting affinity in antibody-engineering strategies (Bostrom *et al.*, 2011; Acchione *et al.*, 2009).

If only one of the different FabA models is used as a reference for comparison with previous solved FabG counterparts, including the human FabG reported here, several differences appear. Nevertheless, we have determined the FabA structure in three different crystal forms, one of which includes two Fabs in the asymmetric unit. The quantitative comparison (Schneider, 2000) of these four independently refined heterodimers allowed us to exclude most of the small rearrangements that probably result from crystal contact effects. Normal-mode analyses were performed (Delarue, 2008), as well as analysis of the *B*-factor distribution by residue, and did not reveal any significant differences between FabA and FabG when taking all of the models into consideration (data not shown).

However, there are significant differential features that stand out. The hydrophobic core of interacting residues bridging the C_{H1} and V_H domains is present in both IgA1- and IgG-isotype Fabs, but it is clear that that present in FabA is further stabilized both by the fact that Pro122 (which is a Thr in FabG) introduces a strict constraint on the main-chain flexibility within the switch loop and by the added hydrogen bond that directly connects two residues from each domain: Tyr209 in the C_{H1} domain and Leu11 in the V_H domain. This is readily visible on the comparison of the solvent-accessible surfaces, focusing on the switch regions of both IgA1

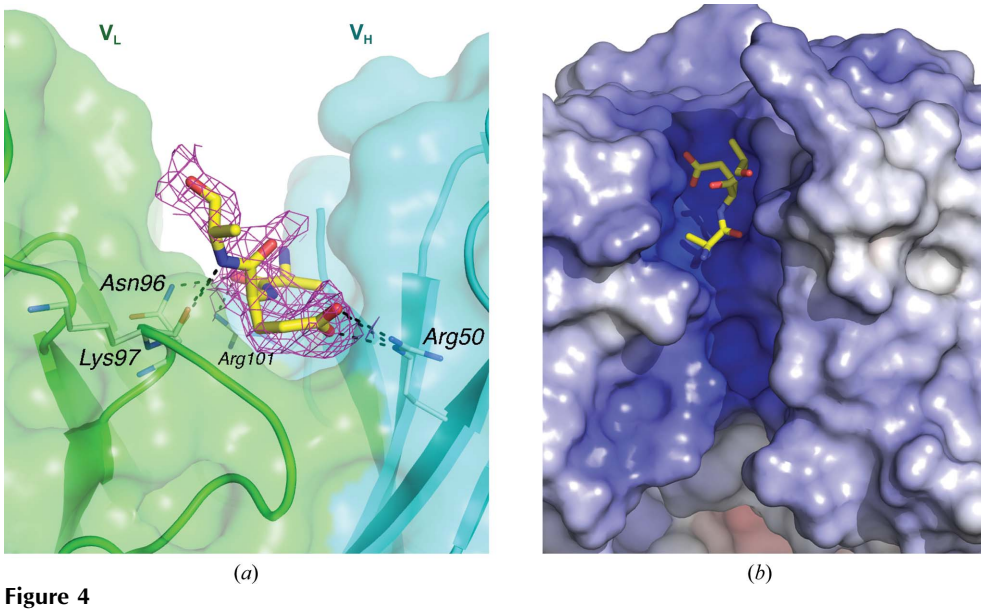

Figure 4
Human IgG1κ Fab in complex with an antigenic peptide. (*a*) σ_A-weighted $2mF_{obs} - DF_{calc}$ electron-density map of FabG contoured at 1σ. For clarity, the map is only shown around the visible residues of the antigenic peptide. Some of the polar interactions with paratope residues are depicted as dashed lines. A detailed description is given in the main text. (*b*) Molecular surface of FabG coloured by electrostatic potential as mapped onto the solvent-accessible surface (colour ramp from $-10k_BT/e_c$ in red to $10k_BT/e_c$ in blue, where k_B is the Boltzmann constant, T is the absolute temperature and e_c is the charge of one electron). The model shown corresponds to the peptide-complexed protein, although the peptide residues were removed for the Poisson–Boltzmann electrostatic potential calculation.

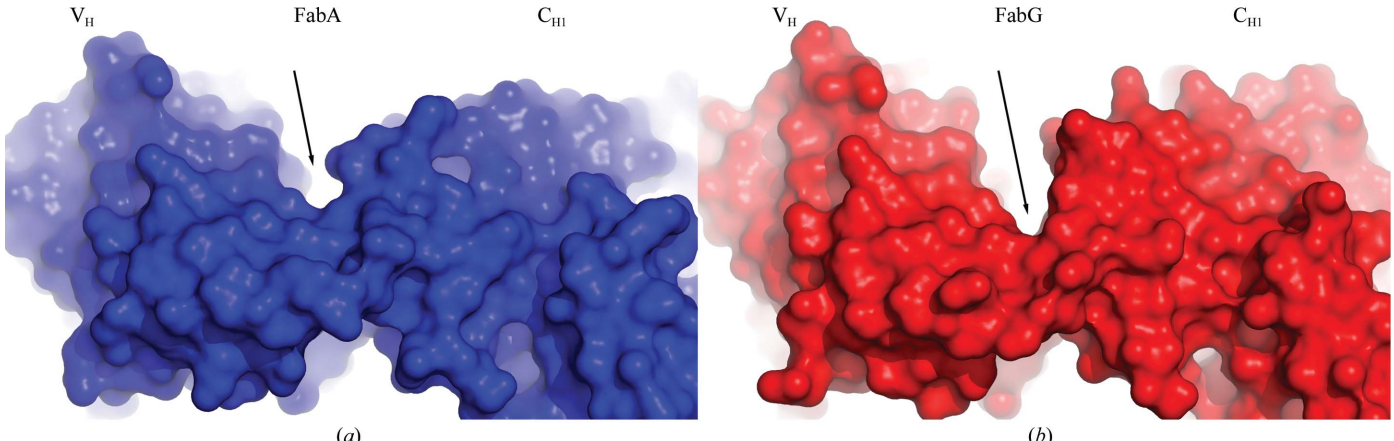

Figure 5
FabA *versus* FabG V_H–C_{H1} interfaces. The solvent-accessible surfaces of (*a*) human IgA1κ FabA and (*b*) IgG1κ FabG are shown in blue and red, respectively. The models are shown in an identical orientation viewed from the heavy-chain side. The arrows highlight the difference in the tightness of interaction between the two domains in the two different Ig isotypes.

and IgG1, in this report (Fig. 5). This prompted us to look at quantitative comparisons of the solvent-accessible volume (Dundas *et al.*, 2006) of the central cavity limited by the four Ig domains in the Fab dimer. Indeed, correlated with the tighter constant–variable interaction, the calculated volumes are consistently smaller in FabA compared with reported FabGs. Taking the average volume among all of the models that we report here, FabA shows a central cavity of 1500 ± 300 Å^3 compared with 3800 ± 500 Å^3 in the related FabG (or 3300 ± 900 Å^3 as calculated from 100 reported FabGs randomly chosen according to differing resolutions, with minimum values not lower than 2400 Å^3). It is pertinent to highlight that this ∼2.5-fold difference holds irrespective of the different crystal-packing environments that are present in the four independently refined FabA heterodimers. However, the lack of redundant data concerning IgA Fabs demands further studies in order to confirm the general validity of this property. The two available three-dimensional models of mouse IgA1 Fab display intermediate values (∼2400 Å^3).

The scenario that emerges from the structural analysis of these human FabA crystallographic models is that overall they are expected to be more rigid than their FabG counterparts. The constant–variable interface displays tighter contacts, which result in a reduced central cavity volume. Some of these features had previously been suggested on the basis of molecular modelling, given that the structure of the IgA1 Fab had not been experimentally determined (Pritsch *et al.*, 2000). A second source of rigidity in the IgA1 Fab results from the presence of an extra inter-chain disulfide bond linking both constant domains. This bond modulates the heavy/light-chain relative orientation, as can be readily observed on comparison with different available FabG1 structures, including the related human monoclonal FabG1 that we have now solved. This provokes a subsequent reduction of the solvent-exposed cavity located at the C_{H1}–C_L interdomain tip. A glimpse into this effect can readily be obtained by comparing the two isotype variants included in this report, where a slight modification of ∼5° in the angle between the C_{H1}–V_H domains (Su *et al.*, 1998) is observed, modifying the V_H–V_L arrangement, a reorganization that, however subtle, may critically influence the antigen-binding paratope (Dam *et al.*, 2008). This angular difference that we are referring to is included in a plane that is orthogonal to that defined according to the canonical elbow angle (Stanfield *et al.*, 2006). This rearrangement could easily transmit conformational information exerting long-distance effects from a more rigid C_{H1} domain through a tight C_{H1}–V_H interface. However, this cannot yet be considered as a conclusive piece of evidence, mainly because of two reasons. Firstly, according to normal-mode analysis simulations the intrinsic angular flexibility within the C_{H1}–V_H plane being considered is predicted to be of the same order as the angle difference actually measured between FabG and FabA. On the other hand, extensive attempts to trap the peptide in complex with the IgA Fab proved unsuccessful, as did attempts to observe a fully occupied antigen-binding crevice in the FabG–peptide complex. Although further structural snapshots might derive a definitive mechanistic description of long-range effects in the determination of antigen-binding properties, recent evidence is indeed consistent with these hypotheses. The secondary structures of mouse IgGs of different isotypes that share identical variable domains undergo different changes upon antigen binding (Janda & Casadevall, 2010). More recently, the C_{H1} region of a human broadly neutralizing anti-HIV-1 antibody has been shown to contribute to shaping its epitope specificity, antibody affinity and functional activities, leading the authors to propose focusing on the induction of both IgA and IgG antibodies for the design of effective anti-HIV vaccines (Tudor *et al.*, 2012).

In combination with information from medium-resolution studies of the IgA Fc region (Herr *et al.*, 2003), together with the low-resolution models of full-length IgAs (Boehm *et al.*, 1999; Furtado *et al.*, 2004; Almogren *et al.*, 2006), we are now contributing a new piece to the puzzle: the antigen-binding region of human IgA1 at near-atomic resolution. Further structural work is clearly needed to accumulate a larger array of IgA and FabA crystallographic models and thus to be able to draw firm conclusions about the particular features that characterize this important class of immunoglobulins. The comparison of two related Fabs in which the only difference resides in the permuted C_{H1} domains does suggest that greater rigidity in the C_{H1}–C_L and the C_{H1}–V_H FabA interfaces may exert long-distance effects including subtle but functionally relevant reorganizations of the paratope of the antibody.

We acknowledge Nicole Larrieux at the Protein Crystallography Facility (PXF), Institut Pasteur de Montevideo for extensive help with crystallization and crystal handling. We are especially grateful to Pamela Bjorkman and Anthony West for providing the source code for their program *Dom_Angle* to calculate inter-domain angular relationships.

References

Acchione, M., Lipschultz, C. A., DeSantis, M. E., Shanmuganathan, A., Li, M., Wlodawer, A., Tarasov, S. & Smith-Gill, S. J. (2009). *Mol. Immunol.* **47**, 457–464.
Adams, P. D. *et al.* (2010). *Acta Cryst.* D**66**, 213–221.
Al-Lazikani, B., Lesk, A. M. & Chothia, C. (1997). *J. Mol. Biol.* **273**, 927–948.
Almogren, A., Furtado, P. B., Sun, Z., Perkins, S. J. & Kerr, M. A. (2006). *J. Mol. Biol.* **356**, 413–431.
Baker, N. A., Sept, D., Joseph, S., Holst, M. J. & McCammon, J. A. (2001). *Proc. Natl Acad. Sci. USA*, **98**, 10037–10041.
Boehm, M. K., Woof, J. M., Kerr, M. A. & Perkins, S. J. (1999). *J. Mol. Biol.* **286**, 1421–1447.
Bostrom, J., Haber, L., Koenig, P., Kelley, R. F. & Fuh, G. (2011). *PLoS One*, **6**, e17887.
Brandtzaeg, P., Baekkevold, E. S., Farstad, I. N., Jahnsen, F. L., Johansen, F. E., Nilsen, E. M. & Yamanaka, T. (1999). *Immunol. Today*, **20**, 141–151.
Chen, V. B., Arendall, W. B., Headd, J. J., Keedy, D. A., Immormino, R. M., Kapral, G. J., Murray, L. W., Richardson, J. S. & Richardson, D. C. (2010). *Acta Cryst.* D**66**, 12–21.
Chi, S.-W., Maeng, C.-Y., Kim, S. J., Oh, M. S., Ryu, C. J., Kim, S.-J., Han, K.-H., Hong, H. J. & Ryu, S.-E. (2007). *Proc. Natl Acad. Sci. USA*, **104**, 9230–9235.
Chintalacharuvu, K. R., Yu, L. J., Bhola, N., Kobayashi, K., Fernandez, C. Z. & Morrison, S. L. (2002). *J. Immunol.* **169**, 5072–5077.

Cooper, L. J., Shikhman, A. R., Glass, D. D., Kangisser, D., Cunningham, M. W. & Greenspan, N. S. (1993). *J. Immunol.* **150**, 2231–2242.
Dam, T. K., Torres, M., Brewer, C. F. & Casadevall, A. (2008). *J. Biol. Chem.* **283**, 31366–31370.
DeLano, W. L. (2002). *PyMOL*. http://www.pymol.org.
Delarue, M. (2008). *Acta Cryst.* D**64**, 40–48.
Dighiero, G., Guilbert, B. & Avrameas, S. (1982). *J. Immunol.* **128**, 2788–2792.
Dundas, J., Ouyang, Z., Tseng, J., Binkowski, A., Turpaz, Y. & Liang, J. (2006). *Nucleic Acids Res.* **34**, W116–W118.
Emsley, P. & Cowtan, K. (2004). *Acta Cryst.* D**60**, 2126–2132.
Furtado, P. B., Whitty, P. W., Robertson, A., Eaton, J. T., Almogren, A., Kerr, M. A., Woof, J. M. & Perkins, S. J. (2004). *J. Mol. Biol.* **338**, 921–941.
Hanson, L. A. & Brandtzaeg, P. (1993). *Immunol. Today*, **14**, 416–417.
Herr, A. B., Ballister, E. R. & Bjorkman, P. J. (2003). *Nature (London)*, **423**, 614–620.
Houdayer, M., Bouvet, J.-P., Wolff, A., Magnac, C., Guillemot, J.-C., Borche, L. & Dighiero, G. (1993). *J. Immunol.* **150**, 311–319.
Inbar, D., Rotman, M. & Givol, D. (1971). *J. Biol. Chem.* **246**, 6272–6275.
Iwasaki, H., Zhang, Y., Tachibana, K., Gotoh, M., Kikuchi, N., Kwon, Y.-D., Togayachi, A., Kudo, T., Kubota, T. & Narimatsu, H. (2003). *J. Biol. Chem.* **278**, 5613–5621.
Janda, A. & Casadevall, A. (2010). *Mol. Immunol.* **47**, 1421–1425.
Kabsch, W. (2010). *Acta Cryst.* D**66**, 125–132.
Kaetzel, C. S. (2005). *Immunol. Rev.* **206**, 83–99.
Kosowska, K., Reinholdt, J., Rasmussen, L. K., Sabat, A., Potempa, J., Kilian, M. & Poulsen, K. (2002). *J. Biol. Chem.* **277**, 11987–11994.
Leslie, A. G. W. (1992). *Jnt CCP4/ESF–EACBM Newsl. Protein Crystallogr.* **26**.
Mariuzza, R. A. & Poljak, R. J. (1993). *Curr. Opin. Immunol.* **5**, 50–55.
Mattu, T. S., Pleass, R. J., Willis, A. C., Kilian, M., Wormald, M. R., Lellouch, A. C., Rudd, P. M., Woof, J. M. & Dwek, R. A. (1998). *J. Biol. Chem.* **273**, 2260–2272.
McLean, G. R., Torres, M., Elguezabal, N., Nakouzi, A. & Casadevall, A. (2002). *J. Immunol.* **169**, 1379–1386.
Mulks, M. H. & Shoberg, R. J. (1994). *Methods Enzymol.* **235**, 543–554.
Poljak, R. J. (1991). *Mol. Immunol.* **28**, 1341–1345.
Pritsch, O., Hudry-Clergeon, G., Buckle, M., Petillot, Y., Bouvet, J.-P., Gagnon, J. & Dighiero, G. (1996). *J. Clin. Invest.* **98**, 2235–2243.
Pritsch, O., Magnac, C., Dumas, G., Bouvet, J.-P., Alzari, P. & Dighiero, G. (2000). *Eur. J. Immunol.* **30**, 3387–3395.
Ramsland, P. A. & Farrugia, W. (2002). *J. Mol. Recognit.* **15**, 248–259.
Ramsland, P. A., Willoughby, N., Trist, H. M., Farrugia, W., Hogarth, P. M., Fraser, J. D. & Wines, B. D. (2007). *Proc. Natl Acad. Sci. USA*, **104**, 15051–15056.
Royle, J. A. (2006). *Biometrics*, **62**, 97–102.
Schneider, T. R. (2000). *Acta Cryst.* D**56**, 714–721.
Segal, D. M., Padlan, E. A., Cohen, G. H., Rudikoff, S., Potter, M. & Davies, D. R. (1974). *Proc. Natl Acad. Sci. USA*, **71**, 4298–4302.
Stanfield, R. L., Zemla, A., Wilson, I. A. & Rupp, B. (2006). *J. Mol. Biol.* **357**, 1566–1574.
Studier, F. W. (2005). *Protein Expr. Purif.* **41**, 207–234.
Su, X.-D., Gastinel, L. N., Vaughn, D. E., Faye, I., Poon, P. & Bjorkman, P. J. (1998). *Science*, **281**, 991–995.
Suh, S. W., Bhat, T. N., Navia, M. A., Cohen, G. H., Rao, D. N., Rudikoff, S. & Davies, D. R. (1986). *Proteins*, **1**, 74–80.
Tonegawa, S. (1983). *Nature (London)*, **302**, 575–581.
Torres, M. & Casadevall, A. (2008). *Trends Immunol.* **29**, 91–97.
Torres, M., Fernandez-Fuentes, N., Fiser, A. & Casadevall, A. (2007*a*). *J. Biol. Chem.* **282**, 13917–13927.
Torres, M., Fernandez-Fuentes, N., Fiser, A. & Casadevall, A. (2007*b*). *PLoS One*, **2**, e1310.
Torres, M., May, R., Scharff, M. D. & Casadevall, A. (2005). *J. Immunol.* **174**, 2132–2142.
Trapani, S. & Navaza, J. (2008). *Acta Cryst.* D**64**, 11–16.
Tudor, D., Yu, H., Maupetit, J., Drillet, A. S., Bouceba, T., Schwartz-Cornil, I., Lopalco, L., Tuffery, P. & Bomsel, M. (2012). *Proc. Natl Acad. Sci. USA*, **109**, 12680–12685.
Tzeng, S. R. & Kalodimos, C. G. (2012). *Nature (London)*, **488**, 236–240.
Winn, M. D. *et al.* (2011). *Acta Cryst.* D**67**, 235–242.
Yoo, E. M. & Morrison, S. L. (2005). *Clin. Immunol.* **116**, 3–10.